Aeroacoustic Testing of UAS-Scale Rotors for a Quadcopter in Hover and Forward Flight

Nicole A. Pettingill, * Nikolas S. Zawodny, † and Christopher S. Thurman, ‡
NASA Langley Research Center, Hampton, VA, 23681

A series of experiments was conducted in an anechoic chamber and wind tunnel to investigate the noise and performance of an optimum hovering rotor design. The optimum hovering rotor experimental data set presented in this paper provides the community with a rotor that is theoretically easier to model. Isolated rotors were tested in an anechoic hover chamber as well as on a representative quadcopter vehicle. In the anechoic chamber, performance and acoustic measurements were taken at various rotor speeds to compare to those of a commercial-off-the-shelf (COTS) rotor. In the wind tunnel, free-stream velocity, vehicle pitch, and rotor rotation rates were varied to achieve various hover and forward flight operating conditions. Previous investigation of a small quadcopter in the Low Speed Aeroacoustic Wind Tunnel (LSAWT) had identified possible broadband and interactional noise sources due to rotor airframe interaction and rotor-rotor interaction. These publications identified separation, turbulent boundary layer trailing edge, and bluntness vortex shedding as the main sources of self-generated airfoil noise. By replacing the COTS rotor with an optimum hovering rotor design, self-generated broadband noise was reduced for both hover and forward flight conditions for isolated rotor runs. However, the optimum rotors only reduced noise levels for full-vehicle hover conditions, and had little to no reduction in full-vehicle forward flight conditions.

Nomenclature

English

c	Chord length, m
$c_\circ$	Ambient speed of sound, m/s
C_T	Rotor thrust coefficient, $T/(\rho\pi\omega^2 R^4)$
f	Frequency, Hz
H	Trailing edge bluntness, m
M_∞	Wind tunnel freestream Mach number
M_{tip}	Hover tip Mach number $\omega_R/c_\circ$
n	Power scaling
N_b	Number of rotor blades
r	Spanwise location from hub, m
R	Blade radius, m
T_v	Vehicle thrust, N
T	Rotor thrust, N
$T*$	Rotor thrust, rel. $\rho_{std} M_{tip}^2$, N

Greek

α_v	Vehicle or rotor hub plane angle of attack, relative to the freestream velocity direction, deg.
$\theta_\circ$	Observer angle, deg.
Θ	Blade pitch angle, deg.
Ω	Rotation rate, RPM
ω	Rotation rate, $\Omega(2\pi/60)$, rad./s
μ	Rotor advance ratio, $M_\infty \cos(\alpha_v)/M_{tip}$
ρ	Atmospheric density, kg/m^3

*Research Aerospace Engineer, Aeroacoustics Branch, AIAA Member; nicole.a.pettingill@nasa.gov
†Research Aerospace Engineer, Aeroacoustics Branch, AIAA Member; nikolas.s.zawodny@nasa.gov
‡Research Aerospace Engineer, Aeroacoustics Branch, AIAA Member; christopher.thurman@nasa.gov

Subscript

bb	Broadband noise
bb, pr	Broadband noise with tonal peaks removed
hc	Observer in hover chamber
$mech$	Mechanical rotation rate
std	Sea level, standard day conditions
wt	Observer in wind tunnel

I. Introduction

Increased demand in advanced air mobility (AAM) has motivated research toward identifying and characterizing the noise sources produced by vehicles such as quadcopters. Wind tunnel tests of small rotors are beneficial in assessing the potential noise impact of both unmanned aerial vehicles (UAVs) and larger urban air mobility (UAM) vehicles. A UAV known as the Straight Up Imaging (SUI) Endurance quadcopter has been tested and modeled extensively. The aerodynamic performance of the SUI quadcopter was tested in the US Army 7- by 10-Foot Wind Tunnel at the NASA Ames Research Center by Iv et al. [1]. The representative quadcopter was then comprehensively modeled by Russell et al. [2], using various inflow models, and it was also computationally modeled by Diaz and Yoon [3] to assess rotor-rotor interactions in hover.

In 2017, a representative vehicle model of the SUI Endurance vehicle was tested in a series of hover and forward flight experiments in the NASA Langley Low Speed Aeroacoustic Wind Tunnel (LSAWT) by Zawodny and Pettingill [4]. The acoustic results of this test were investigated by Pettingill and Zawodny [5], where broadband noise was attributed to interactional and self-generated noise sources. A low-fidelity prediction using the method of Brooks, Pope and Marcolini (BPM) [6] of the broadband noise attributed the self noise to a combination of turbulent-boundary layer (TBL) trailing edge noise, TBL separation noise, and bluntness vortex shedding noise. Additionally, it was found that aft-rotor broadband noise predictions aligned better with experimental data when using a free-wake inflow model in lieu of a uniform inflow model. The results from the investigation in Refs. [4, 5] have motivated a second testing campaign with the objective of reducing noise due to multirotor, rotor-airframe and self-generated noise source mechanisms, and testing simply designed rotors that would theoretically have a uniform inflow. This publication focuses on the acoustic and performance impact of replacing rotor blades on the vehicle, while a second publication [7] will focus on the impact of elevating rotors on interactional noise sources.

In order to move away from commercial-off-the-shelf (COTS) blade designs and explore additive manufacturing techniques, Refs. [8, 9] presented empirical measurements and computational results of an ideally twisted rotor in hover [10]. Rotors with an ideally twisted rotor design were tested in the Small Hover Anechoic Chamber (SHAC) at the NASA Langley Research Center. Advantages of choosing the ideally twisted rotor included easier-to-model uniform inflow properties, as well as the ability to release the geometry to the public.

For the present work, COTS rotors are compared with optimum hovering design rotors by comparing results from isolated rotor hover chamber tests and vehicle-installed rotor wind tunnel tests. The next section describes the representative quadcopter, the COTS and optimum hovering rotors, and the testing facilities. Following this, experimental measurements are presented for hover and forward flight conditions. These results include performance measurements and processed acoustic data acquired for isolated rotors in the hover chamber and vehicle-installed rotors in the wind tunnel. The acoustic and performance impacts of replacing the rotors are discussed, followed by concluding remarks and future work on characterizing the noise mechanisms associated with this vehicle model.

II. Experimental Setup

A. Test Hardware

1. Vehicle

A full-scale representative SUI Endurance vehicle model was tested in the LSAWT. The model, which was the same model tested in Ref. [7], consisted of an airframe, four rotors and their corresponding electric motors. A schematic of the four vehicle-installed rotors and their rotational directions is illustrated in Fig. 1.

The vehicle is equipped with four COTS rotors, each with a radius of 190.5 mm. All rotors counterrotate relative to the neighboring rotors. The front rotors are denoted as R1 and R2, whereas the aft rotors are denoted as R3 and R4. The hub-to-hub distance is approximately 510 mm to neighboring rotors. This vehicle uses fixed-pitch control, meaning that rotor rotation rates are trimmed to achieve different flight conditions. The resulting rotor tip Mach numbers ranged from 0.2 to 0.3, and will be presented in a later section of this publication.

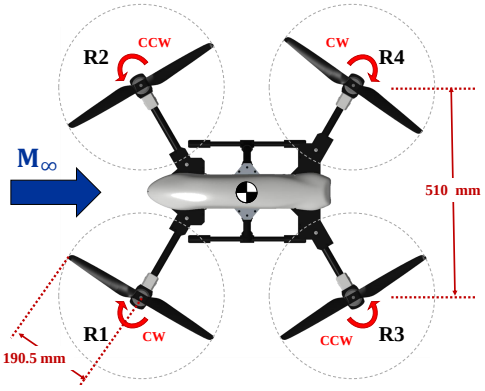

Fig. 1 CAD Model of SUI Endurance Vehicle.

2. Rotors

Three different two-bladed rotors were tested in this investigation. These rotors consisted of a COTS rotor and two optimum hovering rotors. The COTS rotor, shown in Fig. 2(a), is a 381 mm diameter, carbon fiber, single-piece T-Motor CF 15x5 rotor. The optimum hovering rotor, shown in Fig. 2(b), was designed using analytical equations from Ref. [10] and manufactured by ProtoLabs [11]. The optimum design was used for two blade sets, each made of different materials, which are described in more detail in Ref. [8]. The first blade set shown in Fig. 2(c), was made of an "ABS-Like" material manufactured via stereolithography (SLA) [12]. These SLA blades were gritted with .01 inch glass beads along the quarter-chord location of the blade suction side to create a "trip," which prevented laminar boundary layer vortex shedding behavior [13]. This blade set will hereby be denoted as "SLA-gritted" or "SLAg." The second blade set, in Fig. 2(d), was manufactured via the selective laser sintering (SLS) of a material called PA-12, which is a 25% mineral-filled nylon material [14]. These blades will be denoted as "SLS." Both optimum design blade sets utilized a "clam-shell" hub that was designed in-house and fabricated from a clear "PC-like" material [15].

(a) T-Motor COTS Rotor

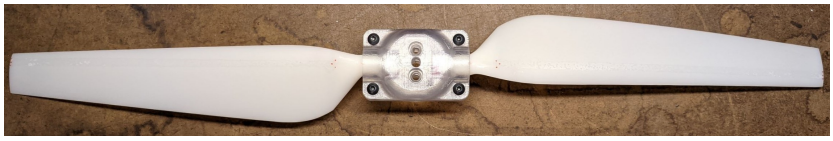

(b) Optimum design rotor

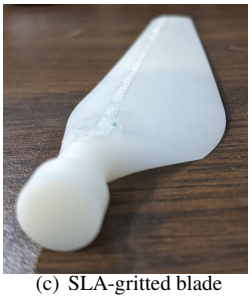

(c) SLA-gritted blade

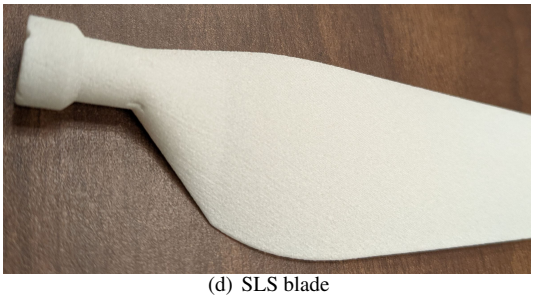

(d) SLS blade

Fig. 2 Images of COTS and optimum rotor blade sets, which were tested in the SHAC and LSAWT.

The COTS blades have a continuously varying airfoil profile along the span. Reference [2] published some geometric properties as well as 3-D laser scans of the airfoils at different spanwise locations. The optimum hovering rotor blades are designed with the same radius, R = 190.5 mm, as the COTS blades. The rotor blade sections had an NACA 5408 airfoil profile along the entire span, which is similar in shape to the airfoil profile of the COTS blades at 80% span. The rotor was designed to generate 8.34 N of thrust at a tip Mach number of M_{tip} = 0.2316 (3950 RPM_c). The mass of the COTS rotor, including the motor mounting disk pictured in Fig. 2(a), is 31 grams.

Table 1 Optimum design parameters.

	Parameter	Value
Geometry	R (mm)	190.5
	c_{tip} (mm)	19.05
	$c(r)$	$\frac{c_{tip}}{r}$
	$H(r)$	$.03c(r)$
Operating Condition	C_T	0.0096
	M_{tip}	0.2316

The optimum hovering rotor blades have a linear chord distribution, since an optimum chord distribution is not physically realizable [13]. The twist distribution results in a minimum induced power requirement, and the taper distribution results in a minimum profile power requirement. Using the clam-shell hub, the blades were set so that the pitch angle at the 0.2R span location was $\Theta = 22.4°$. The mass of the SLA-gritted and SLS rotors, including the clam-shell hub pictured in Fig. 2(b), are both 58 grams. Some design parameters and conditions for the rotor in this study are summarized in Table 1. However, more detailed information on the geometry and design of this optimum hovering rotor blade set is described in Ref. [13].

B. Hover Chamber Test Setup

The three rotors were tested in the hover chamber. A schematic and photograph of the setup are shown in Fig. 3. The SHAC is acoustically treated down to 250 Hz and has working dimensions of 3.87 m x 2.56 m x 3.26 m. The test setup in the SHAC was similar to that of Ref. [8]. A Brüel & Kjær (B&K) LAN-XI data acquisition (DAQ) and BK Connect software system were used for data acquisition. Six B&K Type 4939 and two B&K Type 4954B free-field microphones are located in the upper corner of the SHAC, and span a range of +38° above the plane of the rotor to −50° below the plane of the rotor. They are shown in the diagram in Fig. 3(a). These microphones are located at a minimum of 10 rotor radii away from the rotor, which is in the geometric far-field. A laser sensor tachometer located directly below the rotor was used to monitor the rotation rate of the rotor, and a 6-component AI-IA mini40 multiaxis load cell was used to measure the aerodynamic forces. Each rotor was powered using a KDE Direct 3510 XF 475 KV brushless motor and a 40A optoelectronic speed controller. A photograph of the mounted rotor in the SHAC is shown in Fig. 3(b).

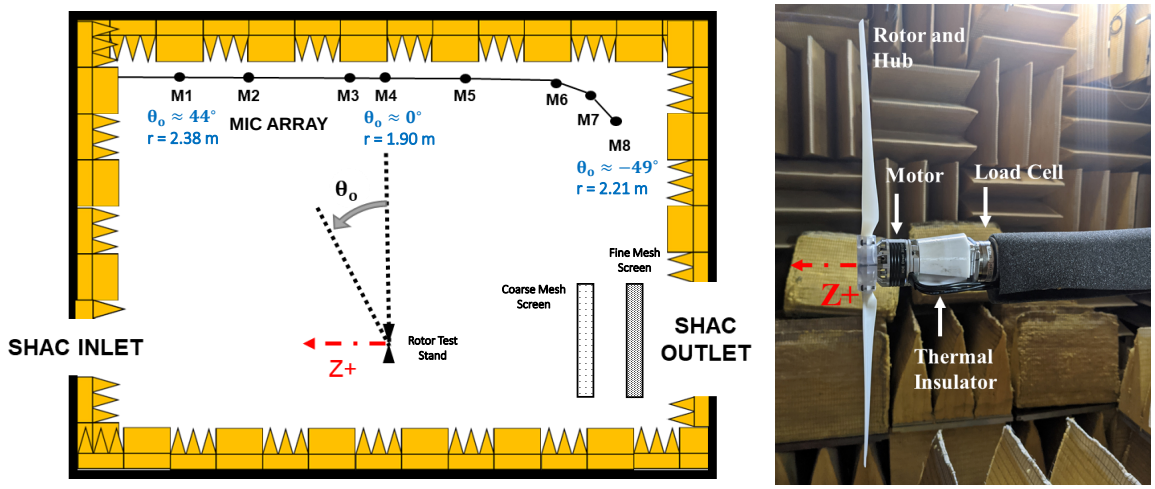

(a) Top view of SHAC facility (not to scale)

(b) Rotor mounted on test stand

Fig. 3 SHAC facility and acoustic measurement configuration.

C. Wind Tunnel Test Setup

The rotors were installed on the representative quadcopter, which was tested in the wind tunnel. The LSAWT is an open-circuit free jet wind tunnel with a test section 5.6 m in length and 1.93 m in inlet diameter. It is acoustically treated down to a cutoff frequency of 250 Hz. Acoustic measurements were taken with a 28 microphone linear array of B&K Type 4939 free-field microphones. As seen in Figs. 4(a) and 4(b), the linear microphone array was located in the upper corner and oriented in line with the streamwise direction. More details on this facility are described in Ref. [4]. Schematics of the microphone locations and vehicle model are found in Figs. 4(c) and 4(d). The vehicle was only tested in one vehicle orientation, the upright position. The upright position results in the linear array of microphones having a "bird's eye" location at $\phi = 140°$, as seen in 4(c). In the 2017 test presented in Ref. [4], A-weighted overall sound

pressure levels between the upright and inverted vehicle orientations only varied < 1 dBA and < 1.5 dBA for forward flight and hover vehicle conditions, respectively. Additionally, hover measurements for observers located between $75° \leq \theta_o \leq 115°$, were contaminated by downwash when the vehicle wasin the overhead position. The decision to only maintain the upright position was made because of load cell installation requirements, as well as data acquisition requirements.

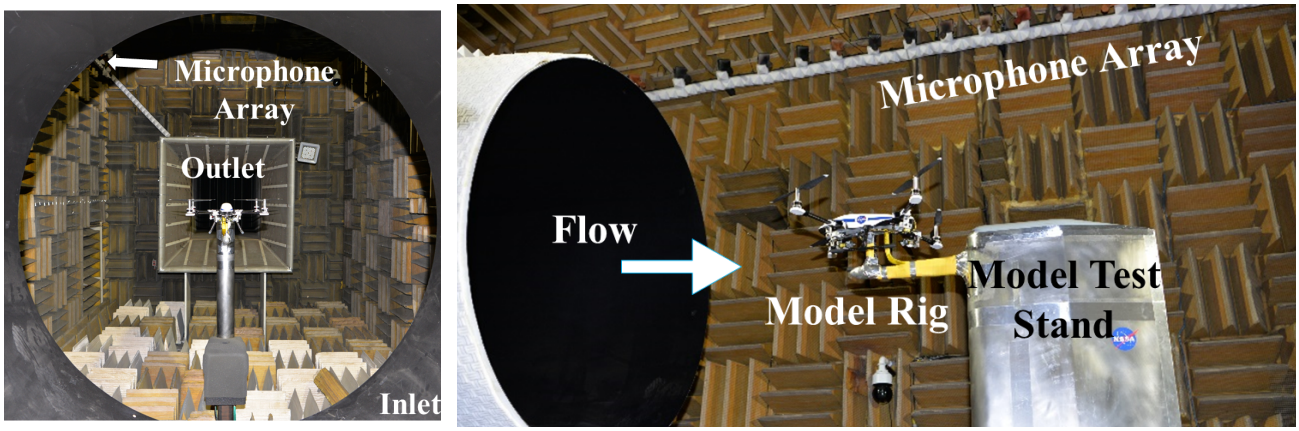

(a) SUI Endurance vehicle mounted on the MTS in upright position.

(b) SUI Endurance vehicle mounted on the MTS.

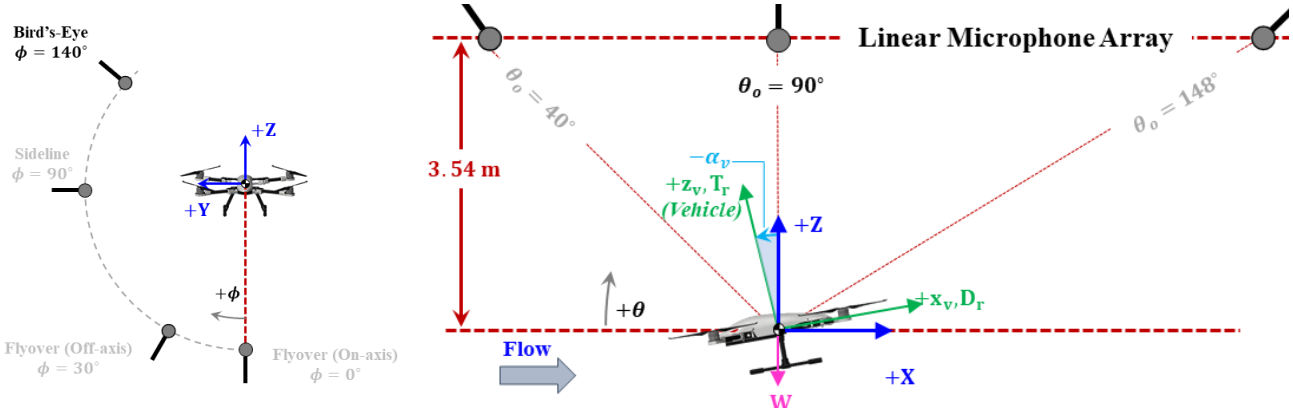

(c) Azimuthal Orientations.

(d) SUI Endurance vehicle mounted on the MTS.

Fig. 4 SUI Endurance vehicle mounted on the Model Test Stand (MTS).

Wind tunnel speed, vehicle pitch, and rotor rotation rates were varied to achieve various hover and forward flight operating conditions. Performance and acoustics measurements were acquired for 27 N, 36 N, and 45 N vehicle thrust conditions. The wind tunnel freestream velocity was varied from $0.0 \leq M_\infty \leq 0.065$. The vehicle pitch was set to $\alpha_v = 0°, -4°$, and $-10°$. As with the previous test in Refs. [4, 5], various model configurations were tested, including: individual rotor, simultaneous rotor pair, and full-vehicle operation configurations. Additional model configurations for the current test include changing out the rotors described in Section II.A.2, and various rotor elevation configurations. The rotor elevation configurations will be presented in a companion paper, Ref [7]. Though not illustrated in Fig. 4(b), isolated rotor configurations in forward flight were tested using the same model test stand. More details on the presented model configurations will be explained in the next section.

III. Results

The performance and acoustic measurements presented in this paper consist of three types of model configurations: isolated rotor, vehicle-installed rotor and full-vehicle. Unless explicitly stated otherwise, isolated rotor hover measurements were acquired in the hover chamber, and isolated forward flight measurements were acquired in the

wind tunnel. Vehicle configurations, including individual vehicle-installed rotor measurements, were acquired solely in the wind tunnel, for both hover and forward flight conditions. It is important to note that both front (R1) and aft (R3) vehicle-installed conditions are presented. Additionally, the hover chamber isolated rotor measurements use the counterclockwise rotor R3, while the wind tunnel isolated rotor measurements use the clockwise rotor R1. Only performance data are presented for isolated rotor configurations; while isolated rotor acoustic data are not presented here, they will be analyzed in a future publication to identify scaling behaviors and test out low-fidelity broadband noise prediction capabilities.

For the purposes of this paper, presented acoustic spectra will correspond to an observer located 35° below the plane of the rotor for hover chamber measurements ($\theta_{\circ,\mathrm{hc}} = -35°$). For wind tunnel forward flight measurements, presented acoustic spectra will correspond to the observer located 90° above the wind tunnel horizontal model plane X+ ($\theta_{\circ,\mathrm{wt}} = 90°$). All presented forward flight measurements were conducted at a tunnel freestream Mach number of $M_\infty = 0.046$ and vehicle pitch angle of $\alpha_v = -10°$.

A. Hover Chamber Test

The performance characteristics of the three blade sets were first tested in the SHAC. The time-history data from the TTL tachometer and load cell provided rotor rotation rate and thrust measurements, respectively. To ensure the processed data were free of ramp-up and room recirculation effects, time durations were determined based on a visual inspection of an out-of-plane acoustic spectrogram, as was done in Ref. [8]. Figure 5 compares the three blade sets using thrust coefficient, corrected thrust and power loading. At the design rotor tip speed of $M_{tip} = 0.2316$, the measured thrust coefficients were 9.7% lower than that of the COTS blades for both the SLA-gritted and SLS rotor blades. As in Ref. [16], an atmospheric correction was applied to dimensional thrust and power measurements using ρc^2 to account for atmospheric variation effects. At the optimum hovering rotor design condition of $M_{tip} = 0.2316$, the SLA-gritted and SLS blades produced 9.0% and 7.4% less thrust than the COTS blades, respectively. It is apparent in the power loading comparison that both the optimum hovering rotor blade sets require more mechanical power to achieve the same thrust as the COTS blades. This could be because both blade sets have either a trip or rough surface that results in a turbulent boundary layer. A tripped boundary layer could result in a decrease in rotor performance [17].

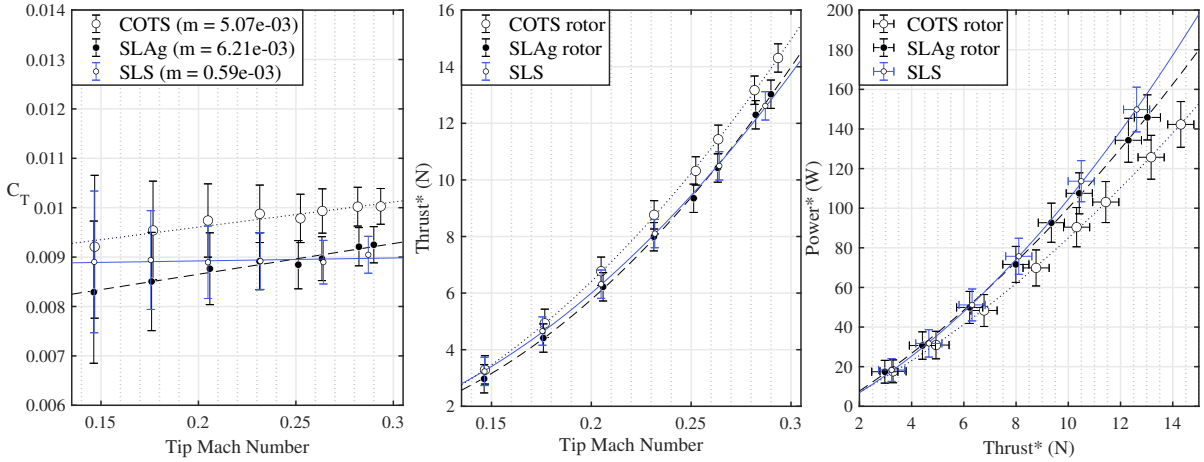

Fig. 5 Performance measurements were taken in the hover chamber for the three blade sets. Thrust coefficient measurements are plotted against rotor tip Mach numbers and first-order curve fits are applied to data (see legend for slopes). Density and speed of sound-corrected thrust and power measurements are plotted, and second-order curve fits are applied to the data.

Acoustic measurements were processed by treating the microphone data as random data sets and computing narrowband acoustic spectra using a Fast Fourier Transform (FFT). For a comparison among the blade sets, resulting spectra were integrated over a range of frequencies between 0.1 kHz ≤ f ≤ 30 kHz for all 8 microphone observers. Figure 6(a) shows the integrated sound pressure levels (denoted as L) of the three blade sets for the $M_{tip} \approx 0.21$ condition. At the out-of-plane observer located −35° below the plane of the rotor, there are noise level reductions of 7.3 dB and 5.7 dB between the COTS blades and the SLA-gritted and SLS blade sets, respectively. A spectral comparison among the

three blade sets can be seen in Fig. 6(b) for the same observer location. The processed data are presented in one-third octave bands, and it is apparent that the optimum blade sets have lower amplitudes at frequencies higher than 500 Hz. Between 4 kHz ≤ f ≤ 16 kHz, the SLA-gritted blades produce lower noise amplitudes than the SLS blades.

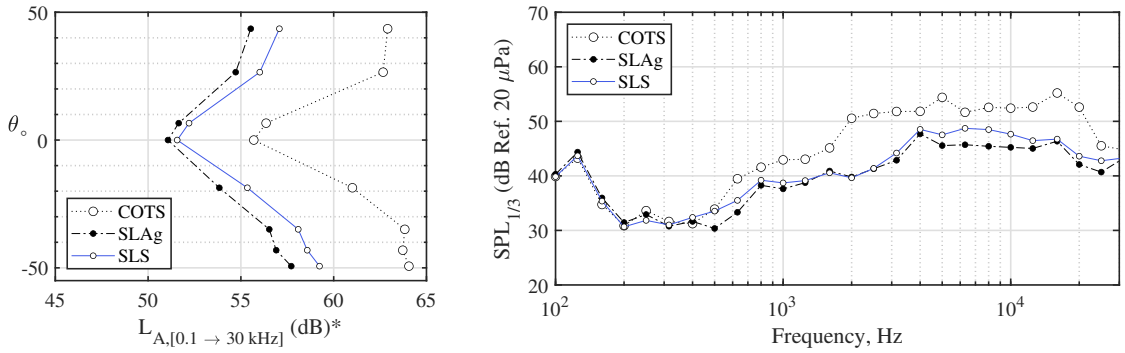

(a) Integrated sound pressure levels*

(b) One-third octave spectra ($\theta_{\circ,hc} = -35°$)

Fig. 6 Acoustic results in the SHAC for the three blade sets ($M_{tip} \approx 0.21$). **Integrated sound pressure levels corrected for a common arc radius of r = 1.9 m.*

B. Wind Tunnel Test

After testing the blade sets in the hover chamber, the rotors were installed on the SUI representative quadcopter for testing in the wind tunnel. The vehicle was pitched forward $\alpha_v = 0°$ and $-10°$, for hover and forward flight conditions, respectively, at three thrust targets: 27 N, 36 N, 45 N. For both the hover and forward flight conditions, 20 seconds of acoustic data were interrogated. The hover data presented in this paper are not free of recirculation effects. Figure 7 compares acoustic narrowband spectra of the baseline installed COTS configuration against those of the previous entry from Ref. [4]. Both hover and forward flight spectra show only minor deviations from the previous test, indicating repeatability of the experiment.

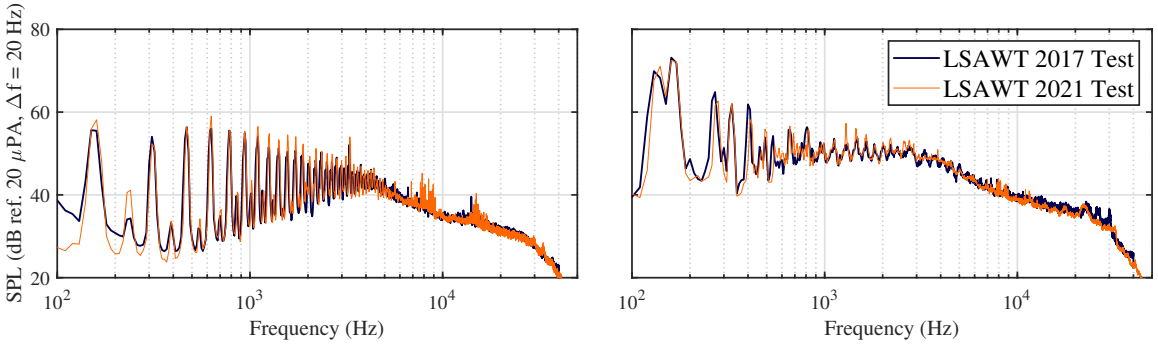

(a) Vehicle in hover ($\alpha_v = 0°$)

(b) Vehicle in forward flight ($\alpha_v = -10°$)

Fig. 7 Comparisons of baseline full vehicle acoustic measurements to those of a previous test (T_v = 45 N, $\theta_{\circ,wt} = 90°$).

1. Hover Performance

With all four rotors installed on the vehicle, rotor rotation rates were trimmed so that the pitch, roll and yaw moments measured by the load cell were nearly zero. A summary of the blade tip speeds required to trim to the three thrust targets in hover is seen in Table 2. For both COTS and SLA-gritted blade sets, trimmed hover conditions resulted in very similar tip Mach numbers for all four rotors, indicating the vehicle is balanced well laterally and axially. Trimmed

hover conditions for the optimum SLA-gritted rotors resulted in faster blade tip speeds of up to 5.3% when compared to the COTS rotors. There are slight deviations in vehicle load cell measurements when compared to the targets. For this paper, all data will be referred to either the vehicle thrust targets of T_v = 27, 36 and 45 N, or as the “low",“medium” or “high" vehicle thrust conditions, respectively.

Table 2 Target vehicle thrust and rotor tip Mach numbers for hover flight conditions.

Thrust (N)		Tip Mach Numbers (COTS/SLAg)			
Target	(Meas. COTS/SLAg)	R1	R2	R3	R4
27 N	(26 N / 26 N)	0.2093 / 0.2195	0.2100 / 0.2205	0.2118 / 0.2226	0.2114 / 0.2200
36 N	(36 N / 35 N)	0.2445 / 0.2527	0.2432 / 0.2503	0.2459 / 0.2527	0.2446 / 0.2505
45 N	(44 N / 44 N)	0.2701 / 0.2812	0.2725 / 0.2813	0.2725 / 0.2811	0.2721 / 0.2816

Individual rotor loads were acquired by removing all but one rotor from the vehicle and taking load cell measurements at the trim tip Mach number conditions defined in Table 2. In hover, the installed rotor thrust is calculated using the load cell measurement of M_y in the $+y_v$ direction and dividing it by the Y distance from the rotor hub center of gravity (i.e., L = 0.2565m). Thrust was calculated in this manner to account for the compliance in the vehicle arm, as explained in Ref. [5]. While Ref. [5] only used this calculation for forward flight thrust measurements, this paper will use it for hover as well, as degradation over time has increased the compliance in the vehicle arm. Figure 8 compares the COTS front rotor (R1) performance measurements to those of the 2017 isolated rotor data acquired in the wind tunnel [5] and the recent measurements acquired in the hover chamber. The thrust coefficients, corrected thrust and torque are shown here. The thrust coefficients of the installed rotors are 6.5% to 5% lower than the thrust coefficient of the isolated rotor in the tunnel. Although not shown here, the SLA-gritted rotors also had reduced thrust coefficent values when they were installed compared to when they were isolated. It is apparent that the recent hover chamber thrust and torque measurements agree well with those of the isolated rotor wind tunnel data from Ref. [5], indicating the hover chamber tests are sufficient for assessing the rotor performance of these rotors in the wind tunnel. The vehicle-installed R1 rotor does generate less thrust at the faster tip speeds than the two isolated rotor cases. This was not the case in Ref. [5], and this could be attributed to the degradation of the vehicle joints and hardware.

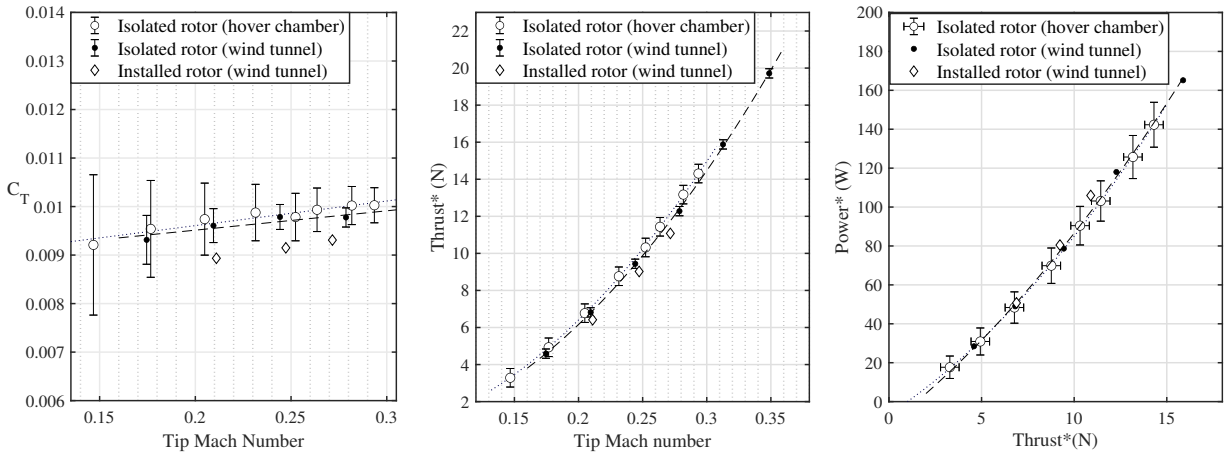

Fig. 8 Performance measurements for COTS rotors in hover (isolated and vehicle-installed).

2. Hover Acoustics

Figure 9 provides an acoustic comparison between the COTS rotors and the SLA-gritted rotors installed in full-vehicle configurations for the low, medium and high vehicle thrust targets (T_v = 27 N, 36 N and 45 N). Figure 9(a) compares the integrated noise levels, both unweighted and A-weighted, of the two blade set configurations, while Fig. 9(b) compares the narrowband spectra at the overhead observer of $\theta_{\circ,wt} = 90°$. For the lowest thrust condition (T_v = 27 N) shown

in Fig. 9(a), both the unweighted and A-weighted noise levels are reduced at all observers, by an average of 4.2 dB and 3.7 dBA, respectively, when SLAg blades are installed. This reduction in noise decreases with increasing thrust condition, as seen in the comparisons at the medium and high thrust conditions (T_v = 36 N, 45 N). At the highest thrust condition, the difference in all levels decreases slightly for observers located upstream of the vehicle at $\theta_{\circ,wt} < -60°$ and downstream $\theta_{\circ,wt} >= 120°$. At the overhead observer ($\theta_{\circ,wt} = 90°$), replacing the COTS rotors with SLA-gritted rotors results in 3.9, 2.3 and 1.1 dB unweighted noise level reductions and 3.4, 1.8 and 0.7 dBA A-weighted noise level reductions, for the low, medium and high thrust conditions, respectively. When examining the spectral comparisons in Fig. 9(b), high frequency broadband noise is reduced for all three thrust conditions, above frequencies of 4, 7 and 9 kHz, for the low, medium and high thrust conditions, respectively. All three thrust conditions have high levels of motor noise at high frequencies when the COTS rotors are installed; for example, at the low thrust conditions the spikes are between 7 and 9 kHz. This motor noise is greatly reduced when the optimum rotors are installed. For the low thrust condition narrowband comparison, the fundamental Blade Passage Frequency (BPF) and associated harmonics of the SLA-gritted configuration occur at higher frequencies (128 Hz) than those of the COTS configuration (122 Hz), which is due to faster blade tip speeds when compared to the COTS rotor, as previously mentioned. Despite spinning faster, the amplitudes of second and subsequent BPF harmonics (253 Hz, 356 Hz, 511 Hz, etc.) of the SLA-gritted configuration are lower than those of the COTS configuration. The narrowband comparisons agree with the directivity plots, with the lowest thrust condition having the highest noise reduction. The highest thrust condition shows little to negligible benefit to installing the optimum hovering rotors, especially with A-weighting the data.

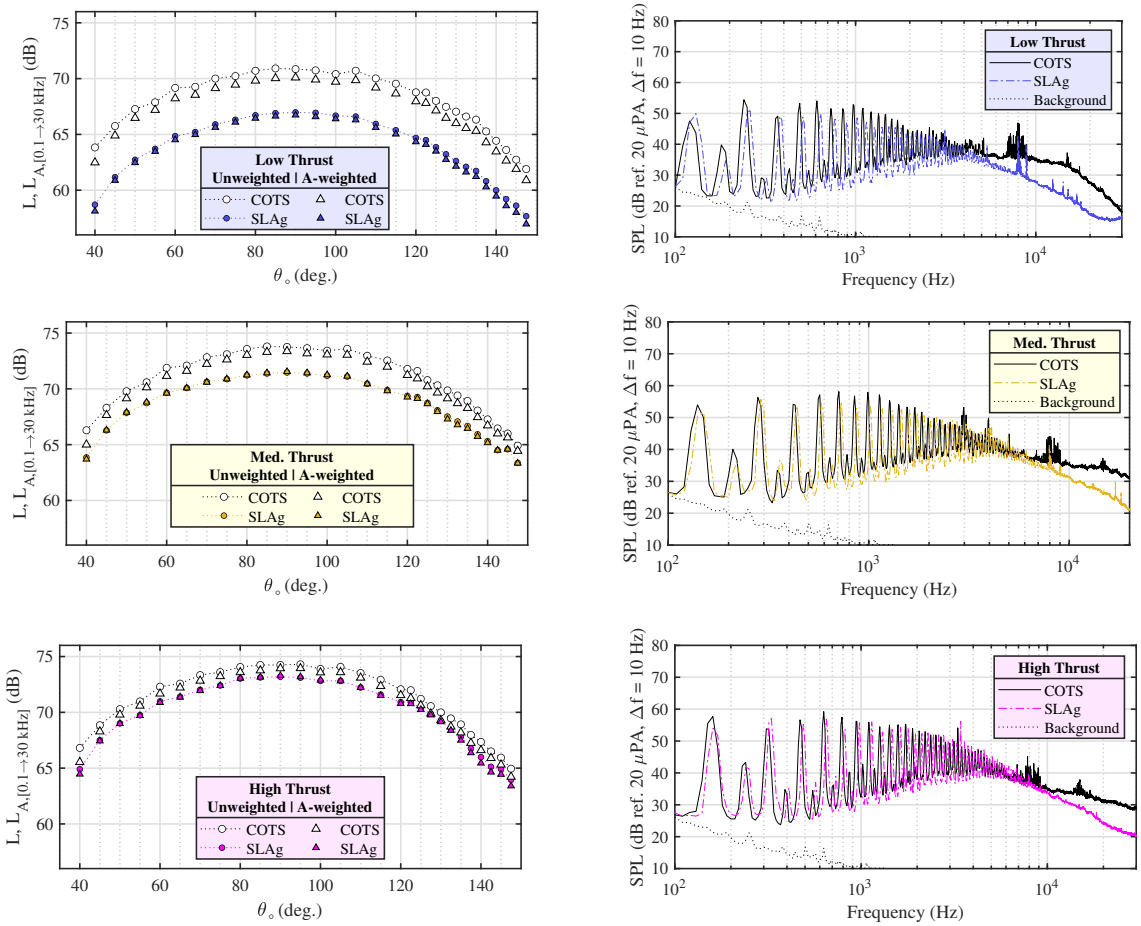

(a) Integrated noise level comparisons

(b) Narrowband spectral comparisons ($\theta_{\circ,wt}$ = 90°)

Fig. 9 Acoustic comparisons between COTS blade and SLA-gritted optimum blade sets installed on the full vehicle in hover for the low, medium and high vehicle thrust conditions (α_v = 0°, M_∞ = 0.0).

Acoustic measurements were taken for the individual rotors when installed on the vehicle. Figure 10(a) provides both unweighted and A-weighted directivities with rotor blade replacement for the lowest thrust condition (T_v = 27 N). It is apparent the configuration with the SLAg rotor is quieter than the configuration with the COTS rotors, with the observer at $\theta_{\circ,\mathrm{wt}} = 90°$ showing unweighted and A-weighted noise level reductions of 3.3 dB and 2.8 dBA, respectively. This condition, along with the two other thrust conditions are presented in Fig. 10(b) as the change in unweighted and A-weighted directivities with rotor blade changes. The low thrust condition provided the best comparison, as higher conditions were more contaminated by motor tones and recirculation effects.

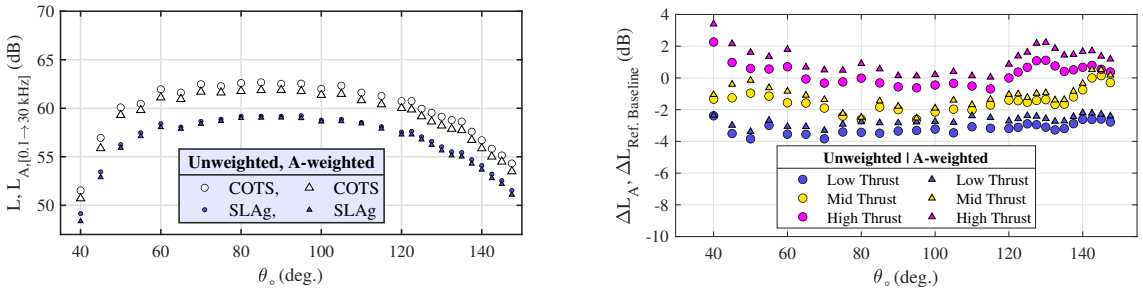

(a) A-weighted directivity comparison for 27 N condition

(b) Change in directivity levels for all three conditions

Fig. 10 Hover acoustic comparisons between COTS and SLAg rotors installed as an individual front rotor (R1) on the vehicle ($\alpha_\mathbf{v} = 0°$, $\mathbf{M}_\infty = 0$).

Spectral comparisons for the low thrust condition are presented in Fig. 11 for the $\theta_{\circ,\mathrm{wt}} = 90°$ observer. Periodic averaging was used to separate the tonal and broadband noise contributions for a given observer; this processing technique is described in Refs. [4, 5]. However, this processing technique is difficult to implement in hover, due to recirculation and turbulence ingestion. Figure 11(a) compares raw spectra and extracted BPF amplitudes for the low thrust condition. At this low thrust condition, the tunnel background noise does affect measurements at frequencies below approximately 400 Hz, and frequencies above 20 kHz. Figure 11(b) compares extracted broadband spectra between 0.4 kHz ≤ f ≤ 20 kHz. To highlight the spectral "shelf", the peaks are removed, as they were in Ref. [8]. The wind tunnel background noise is removed on a pressure basis from all the curves in Fig. 11(b).

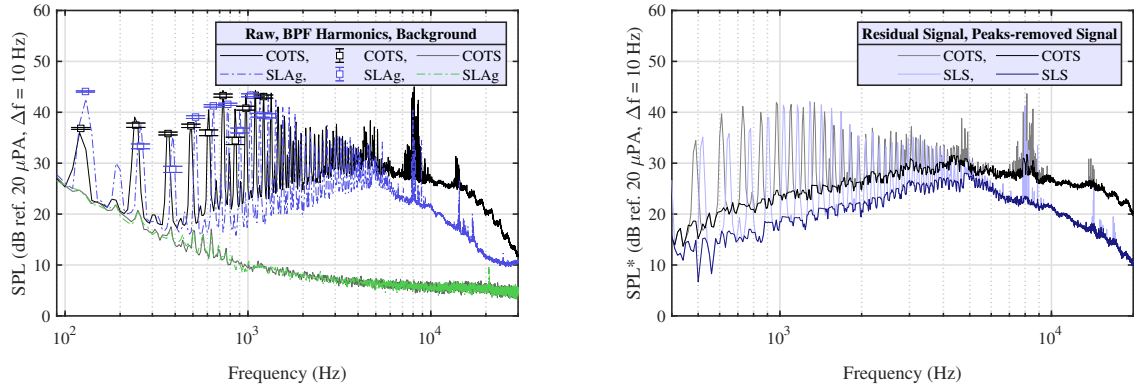

(a) Raw spectra

(b) Broadband spectra

Fig. 11 Hover acoustic comparisons between each of the three blade sets installed as an individual front rotor (R1) on the vehicle for the low vehicle thrust condition ($\mathbf{T_v = 27}$ N, $\alpha_\mathbf{v} = 0°$, $\mathbf{M}_\infty = 0$, $\theta_{\circ,\mathbf{wt}} = 90°$).

Figure 12 provides an acoustic comparison of three aft rotor (R3) configurations with the COTS, SLA-gritted, and SLS rotors installed. The SLS configurations in hover were only tested for the aft R3 rotor, which is why it was chosen for this comparison. Integrated levels are compared for both the lowest (T_v = 27 N) and the highest (T_v = 45 N) trim

conditions for the three rotors in Fig. 12(a). The SLA-gritted configurations have lower noise levels than the SLS blades, especially at the highest thrust condition. However, at the lower thrust condition, both optimum hovering rotor configurations have similar levels. Figure 12(b) shows spectral comparisons for the low and high thrust target conditions (T_v = 27 N and 45 N). At frequencies higher than 5 kHz, the two optimum blade sets have lower noise levels than the COTS blade set for the low thrust condition. The SLA-gritted and SLS blade sets have similar spectral content when compared with each other. As mentioned earlier, the lowest thrust condition is believed to be the least affected by the degradation of the vehicle over time. Because the SLA-gritted rotors generated the least noise in both the hover chamber and wind tunnel tests, those were initially intended to be used for the rest of the test. However, when mounted on the vehicle, there were indications of vibration when monitoring the load cell and visually watching the rotors spin up. The minimal differences in acoustics between the SLA-gritted and SLS blades at this low thrust condition allow for the interchangeability of these blade sets for the rest of this paper.

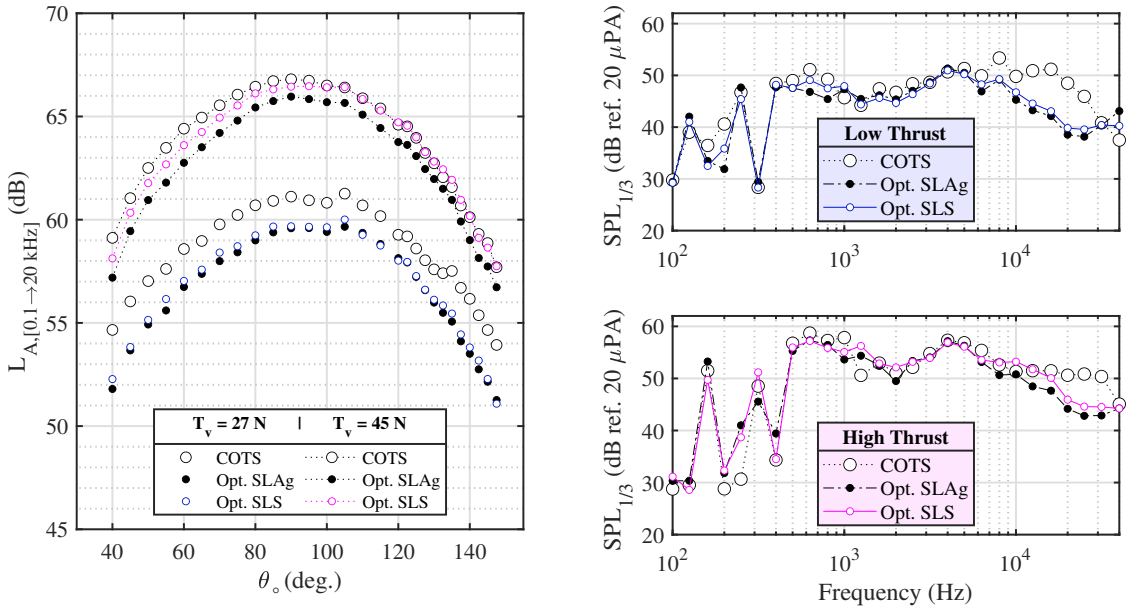

(a) Integrated sound pressure levels comparisond

(b) One-third octave spectral comparisons ($\theta_{\circ,\mathbf{wt}}$ = 90°)

Fig. 12 Acoustic comparison among various blade sets vehicle-installed as an aft rotor (R3) in hover for low and high vehicle thrust conditions (T_v = 27 N, 45 N, α_v = 0°, M_∞ = 0).

3. Forward Flight Performance

The vehicle was pitched $\alpha_v = -10°$ for forward flight measurements, and both COTS and SLS rotors were installed and tested. A summary of the tip Mach numbers required to trim the vehicle to the thrust target is seen in Table 3. When the vehicle was trimmed with the optimum hovering design SLS rotors, they were required to spin up to 4.2% faster than the COTS rotors to achieve the same vehicle thrust. Both rotor test cases had a split between the forward and aft rotor rotation rates, with aft rotors exhibiting higher rotation rates. When the COTS rotors were placed on the vehicle, the tip Mach numbers of the two forward rotors (R1&R2) were very similar to each other, as were the tip Mach numbers of the aft rotors (R3&R4). This indicates the vehicle was well balanced laterally. The increase in aft rotor tip speed was consistent throughout the different thrust target conditions. When the SLS rotors were placed on the vehicle, the starboard rotors (R2&R4) were spinning up to 2.3% faster than the port rotors (R1&R3) for all but one aft pair condition at the highest thrust target. Furthermore, for this condition the port side showed less of a tip speed difference than the starboard side. This could be indicative of slight torsion. These differences are less pronounced at the lower tip speed conditions, but they are indicative of the challenges with trimming the SLS rotors.

Table 3 Target vehicle thrust and rotor tip Mach numbers for forward flight conditions.

Thrust (N)		Tip Mach Numbers (COTS/SLS)			
Target	(Meas. COTS/SLS)	R1	R2	R3	R4
27 N	(28 N / 28 N)	0.1871 / 0.1877	0.1871 / 0.1915	0.2193 / 0.2242	0.2200 / 0.2293
36 N	(37 N / 37 N)	0.2137 / 0.2150	0.2124 / 0.2208	0.2523 / 0.2606	0.2531 / 0.2641
45 N	(46 N / 46 N)	0.2371 / 0.2402	0.2371 / 0.2402	0.2831 / 0.2911	0.2827 / 0.2829

In addition to full vehicle tests, both the COTS and SLS rotors were tested in an isolated rotor configuration. The rotors were pitched forward $\alpha_v = -10$ deg. and spun up to tip speeds ranging from $M_{tip} = 0.1500$ to $M_{tip} = 0.3000$. Figure 13 compares the wind tunnel performance measurements between the COTS and SLS isolated rotors. The thrust coefficients of the SLS rotor have a larger decreasing slope than those of the COTS rotor; this contrasts with hover results presented earlier Fig. 5, where the SLS rotor had an almost negligible slope. There is agreement between the dimensional thrust comparison of the two rotors; however, the power loading comparison shows the SLS rotor performs worse with increasing thrust, with the SLS rotors requiring up to 18.5% more power to achieve the same thrust as the COTS rotors.

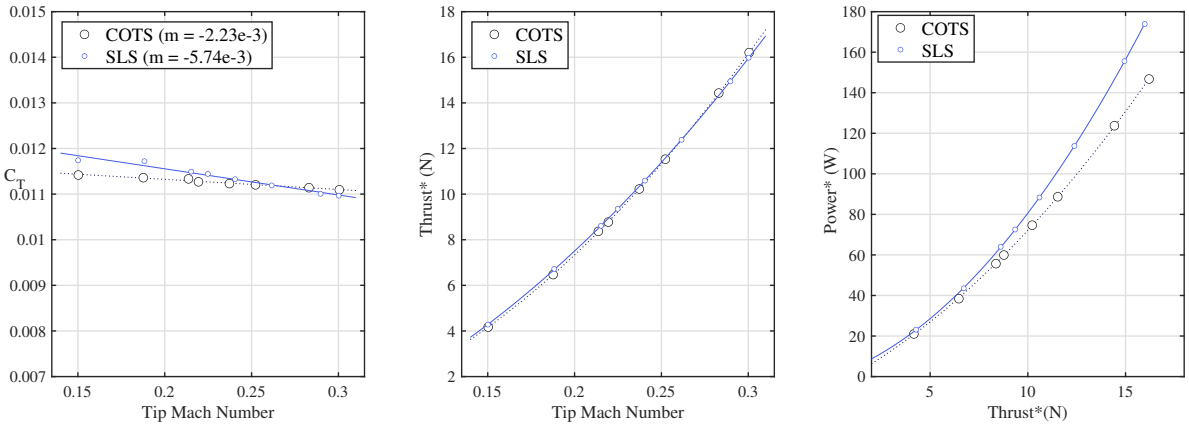

Fig. 13 Performance measurements for isolated COTS and SLS rotors in forward flight. ($\alpha_v = -10°$, $M_\infty = 0.046$).

4. Forward Flight Acoustics

The acoustic characteristics of the two blade sets in forward flight are first evaluated through comparisons of both overall sound pressure levels and acoustic spectral content. Figure 14 provides a full-vehicle acoustic comparison between the COTS blades and the SLS blades installed on the vehicle in forward flight at two thrust conditions. At the low thrust condition of $T_v = 27$ N, replacing the COTS rotors with the SLS rotors shows negligible reduction (< 1dB) when comparing the overall sound pressure levels of the two configurations. At the higher thrust condition of $T_v = 45$ N, replacing the COTS rotors with the SLS rotors actually increases the noise levels, especially at the upstream and downstream observers. However, at the overhead observer of $\theta^\circ_{\circ,wt} = 90°$, this increase is negligible.

Figure 15 shows an acoustic comparison between the COTS and SLS installed on the vehicle as R1 for the low and high vehicle thrust target conditions ($T_v = 27$ N and 45 N). Figure 15(a) provides a comparison of A-weighted OASPL directivities between the COTS and SLS blade sets. There is a maximum noise reduction of up to 4 dB when the COTS rotor is replaced with an optimum SLS rotor. The microphones upstream of the vehicle ($\theta_{\circ,wt} < 90°$) measured larger differences in noise than the microphones downstream of the vehicle. Figure 15(b) provides a comparison of the total noise spectra of the two R1 cases for the observer located directly above the vehicle, $\theta_{\circ,wt} = 90°$. It is observed that noise levels start to decrease at frequencies higher than f = 1kHz. For both cases, there is a presence of motor tones in the frequency range of 7 kHz $\leq$ f $\leq$ 9 kHz.

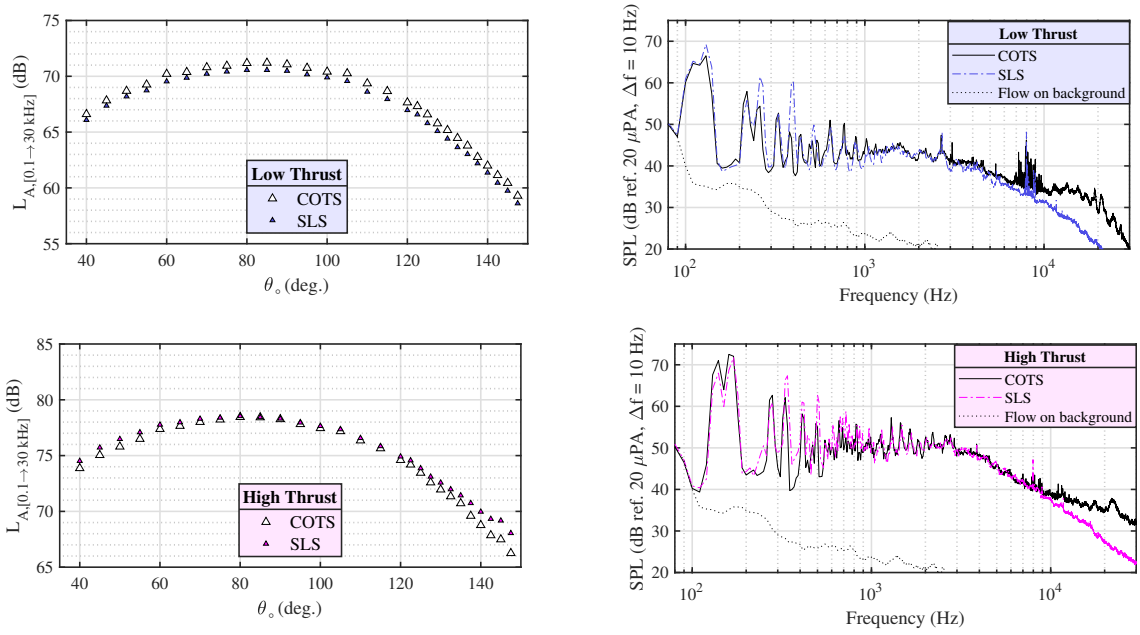

(a) Integrated noise level comparisons

(b) Narrowband spectra comparisons

Fig. 14 Integrated noise level comparisons between COTS and SLS rotors installed on a full vehicle configuration in forward flight at the low and high vehicle thrust conditions (T_v = 27 N, 45 N, $\alpha_v = -10°$, $M_\infty = 0.046$).

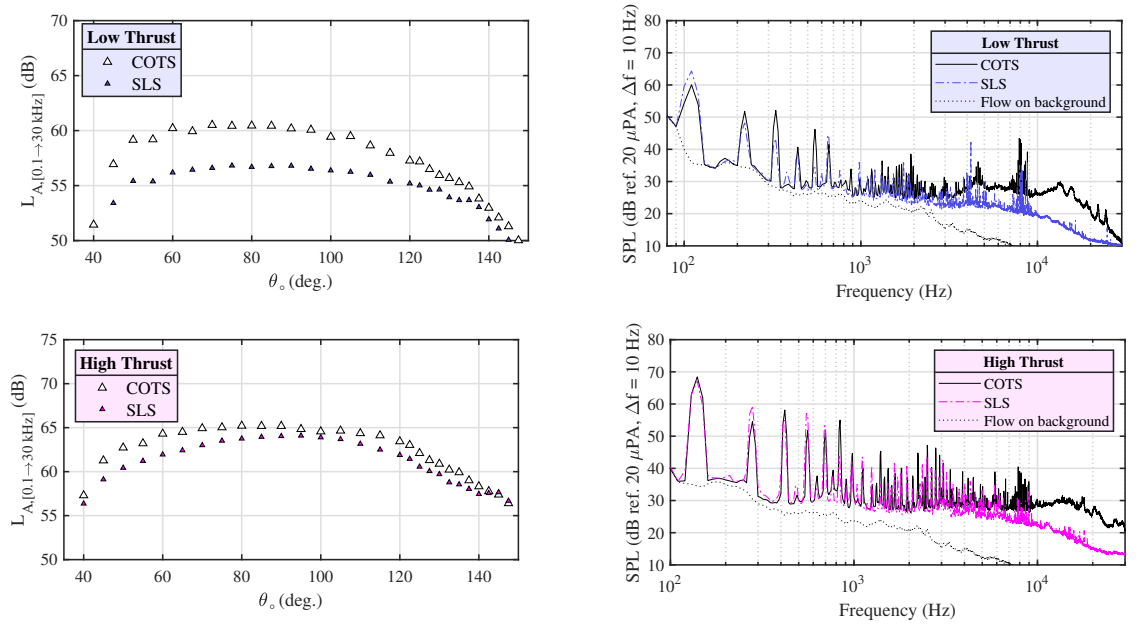

(a) Integrated noise level comparison

(b) Narrowband spectra comparison

Fig. 15 Total noise contributions for COTS and SLS rotors installed as an individual front rotor (R1) on the vehicle in forward flight ($\alpha_v = -10°$, $M_\infty = 0.046$).

As with hover, tonal and broadband noise contributions were separated using periodic averaging for forward flight. Figure 16 shows the results of applying periodic-broadband extraction to the individual R1 cases of the two different blade sets at the low vehicle thrust condition (T_v = 27 N). Figure 16(a) shows a breakdown of periodic and broadband noise contributions of the COTS case. It is interesting to observe how the noise transitions from being tonal-dominated to broadband dominated at a 1/3rd octave band frequency of 2 kHz. This contrasts with the breakdown of noise contributions for the optimum hovering rotor case in Fig. 16(b), where there is no transition to broadband-dominated

noise, as the broadband noise levels remain flat. The broadband content of both blade sets is compared in Fig. 16(c), where it is apparent that especially at frequencies greater than 1 kHz, the COTS rotor case starts to have higher levels of broadband noise than the SLS rotor case. In Ref. [5], broadband noise for a similar COTS test case as Fig. 16(a) was attributed to the self-generated noise sources in the turbulent boundary layer. Finally, Fig. 16(d) compares the BPF harmonics of the two blade sets. As in the spectral comparison presented earlier in Fig. 15(b) for the low thrust condition, the amplitude of the 1st BPF is increased with the SLS blade set replacement. However, the amplitudes of the 2nd through 5th BPF harmonics are reduced with the SLS blade set replacement.

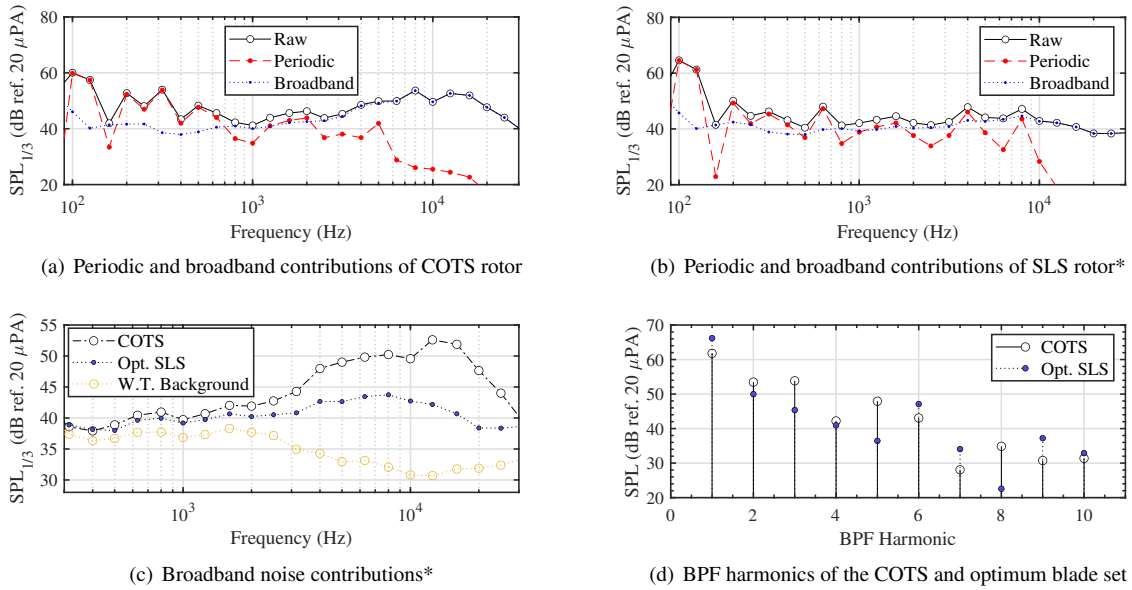

(a) Periodic and broadband contributions of COTS rotor

(b) Periodic and broadband contributions of SLS rotor*

(c) Broadband noise contributions*

(d) BPF harmonics of the COTS and optimum blade set

Fig. 16 Broadband and periodic noise contributions for COTS and SLS rotors installed as an individual front rotor (R1) on the vehicle in forward flight ($\alpha_v = -10°$, $M_\infty = 0.046$). *_Signals are peak-removed spectra_ ($SPL_{bb,pr}$).

Finally, Fig. 17 presents comparisons of the broadband noise contributions at all three thrust conditions. The COTS rotor cases are plotted in Fig. 17(a), and the SLS rotor cases are plotted in Fig. 17(b). The broadband noise levels of the SLS rotors are lower than those of the COTS rotors at the different thrust conditions. The SLS rotors also exhibit a flat behavior across the different frequencies. While these results are indicative of broadband noise trends, a larger range of thrust conditions would be necessary to identify transitional acoustic behavior across various blade tip speeds. While reduction in broadband acoustic content between the tested rotors is very promising, the exact causes of this noise reduction require further data interrogation (i.e., spectral scaling) and consultation of self-noise prediction codes.

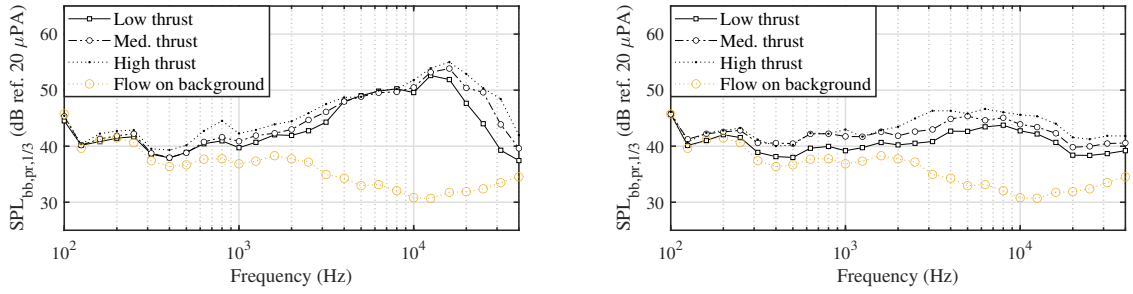

(a) COTS test cases

(b) Optimum SLS test cases

Fig. 17 Broadband noise contributions for the individual front rotor (R1) in forward flight at various thrust conditions ($\alpha_v = -10°$, $M_\infty = 0.046$).

IV. Conclusion and Future Work

Experimental data were acquired in both a hover chamber and a wind tunnel for three rotor blade sets: COTS rotors and two optimum hovering rotors consisting of a boundary layer trip (SLA-gritted) and having noticeable surface roughness caused by the additive manufacturing process used (SLS). Static performance and acoustic measurements of the COTS rotors and the two optimum hovering rotors were acquired in the SHAC and presented in this paper. The SLA-gritted and SLS rotors produced 9.0% and 7.4% less thrust, respectively, than the COTS blades, which was attributed to the turbulent character of the boundary layer of these blade sets [9, 17].

Performance and acoustic measurements of the different rotors in single rotor and full vehicle configurations were acquired in the LSAWT. The vehicle was tested in hover and forward flight conditions for both rotor installation configurations. The baseline acoustic results of the wind tunnel test presented in this paper match those of a previous test entry [5]. Spectral comparisons between vehicle tests installed with COTS rotors and optimum hovering rotors were primarily presented for the low thrust condition (T_v = 27 N), where rotor rig vibrations were minimized. In hover, replacing the COTS rotors with the SLA-gritted optimum rotors on the full vehicle reduced A-weighted noise levels 3.4 dBA and 0.7 dBA for the low and high thrust conditions, respectively. In forward flight, replacing the COTS rotors with the SLS rotors on the full vehicle resulted in negligible changes in noise levels for all tested thrust conditions, since SLS noise levels were lower at high frequencies, where annoyance is low due to being out of the audible hearing range. Hence, the A-weighted directivity plots, which best represent the impact of rotor replacement, only showed a mild reduction in the noise impact of the vehicle. Additionally, there is a presence of rotor/airframe wake ingestion noise, which is independent of the rotor designs [7]. Individual acoustic measurements were examined in hover and forward flight for the front rotor. In hover, changing the COTS rotor to an SLAg rotor resulted in an A-weighted noise level decrease of 2.8 dBA for the low thrust condition and an increase of 0.1 dBA for the high thrust condition. The noise in the low thrust condition was attributed to lower levels in harmonic tones, less broadband noise and less motor noise. In forward flight, changing the COTS rotor with an SLS rotor resulted in A-weighted noise levels that were 3.4 and 1.2 dBA lower for the low and high thrust conditions, respectively.

While these results are indicative of broadband noise trends, a larger range of thrust conditions would be necessary to identify transitional acoustic behavior across various blade tip speeds. Future work includes analysis of higher flow speed and shallower vehicle pitch angle conditions. Future work also includes scaling of acoustic spectra for both hover and forward flight conditions. Broadband noise predictions will also be made, using the semiempirical self-noise prediction methodology devised by Brooks et al. (BPM model) in Ref. [6] and implemented in ANOPP2's Self-Noise Internal Functional Module (ASNIFM) (Ref. [18]). A larger effort should be made on assessing if rotors of this scale can emulate UAM-sized rotors.

The testing of the optimum hovering rotor conducted in this investigation has provided an experimental data set for a rotor whose geometry is more easily distributable and easier to analytically model than a COTS rotor, therefore making the noise signatures of quadcopter configurations such as the SUI Endurance easier to predict. In addition, the replacement of the COTS rotors with the optimum hovering rotors shows promising results in noise reduction. A similar method of noise reduction could be applicable to larger scale UAM vehicles.

Acknowledgments

The authors thank the NASA Revolutionary Vertical Lift Technology (RVLT) project. The authors thank the LSAWT team (John Swartzbaugh, Stan Mason, Jeff Collins, Bryan Lamb, Scott Parks and Jarrett Braxton) who helped with testing in the SHAC.

References

[1] Iv, D. G., Cornelius, J., Waltermire, S., Loob, C., and Schatzman, N. L., "Acoustic Testing of Five Multicopter UAS in the U. S. Army 7- by 10-Foot Wind Tunnel," Tech. Rep. NASA/TM-2018-219894, 2018.

[2] Russell, C. R., Field, M., and Sekula, M. K., "Comprehensive Analysis Modeling of Small-Scale UAS Rotors," *AHS International 73rd Annual Forum*, Fort Worth, TX, May 2017.

[3] Ventura Diaz, P., and Yoon, S., "A Physics-based Approach to Urban Air Mobility," *44th European Rotorcraft Forum*, Delft, The Netherlands, September 2018.

[4] Zawodny, N. S., and Pettingill, N. A., "Acoustic Wind Tunnel Measurements of a Quadcopter in Hover and Forward Flight Conditions," *47th International Congress and Exposition on Noise Control Engineering*, August 2018.

[5] Pettingill, N. A., and Zawodny, N. S., "Identification and Prediction of Broadband Noise for a Small Quadcopter," *Vertical Flight Society International 75th Annual Forum & Technology Display*, Philadelphia, PA, May 2019.

[6] Brooks, T. F., Pope, D. S., and Marcolini, M. A., "Airfoil Self-Noise and Prediction," NASA RP 1218, 1989.

[7] Zawodny, N. S., Pettingill, N. A., and Thurman, C. S., "Identification and Reduction of Interactional Noise of a Quadcopter in Hover and Forward Flight Conditions," *Submission to 51st International Congress and Exposition on Noise Control Engineering*, August 2022.

[8] Pettingill, N. A., Zawodny, N. S., Thurman, C. S., and Lopes, L. V., "Acoustic and performance characteristics of an ideally twisted rotor in hover," *AIAA Scitech 2021 Forum*, Virtual, January 2021. https://doi.org/10.2514/6.2021-1928.

[9] Thurman, C. S., Zawodny, N. S., Pettingill, N. A., Lopes, L. V., and Baeder, J. D., "Physics-informed Broadband Noise Source Identification and Prediction of an Ideally Twisted Rotor," *AIAA SciTech 2021 Forum*, Virtual, January 2021.

[10] Leishman, J. G., *Principles of Helicopter Aerodynamics*, Cambridge University Press, New York, NY, 2000.

[11] Protolabs, "Proto Labs, Inc." https://www.protolabs.com/, 2022. Accessed January 10, 2022.

[12] Protolabs, "Stereolithography ABS-Like White Material Data Sheet," https://www.protolabs.com/media/yg2nlbh4/sla-accura-xtreme-white-120721.pdf, January 2022. Accessed January 10, 2022.

[13] Thurman, C. S., Zawodny, N. S., and Pettingill, N. A., "The Effect of Boundary Layer Character on Stochastic Rotor Blade Vortex Shedding Noise," *The Vertical Flight Society's 78th Annual Forum and Technology Display*, Fort Worth, TX, May 2022.

[14] Protolabs, "Selective Laser Sintering PA 12 Mineral-Filled Material Data Sheet," https://www.protolabs.com/media/rgtpv4se/sls-pa-12-mineral-filled-120821.pdf, January 2022. Accessed January 10, 2022.

[15] Protolabs, "Stereolithography PC-Like Translucent Material Data Sheet," https://www.protolabs.com/media/1021641/sla-data-sheet-accura-60-f.pdf, December 2019. Accessed January 10, 2022.

[16] Whiteside, S., Zawodny, N., Fei, X., Pettingill, N. A., Patterson, M. D., and Rothhaar, P., "An Exploration of the Performance and Acoustic Characteristics of UAV-Scale Stacked Rotor Configurations," *AIAA Scitech 2019 Forum*, San Diego, CA, Jan. 2019.

[17] Abdel-Rahman, A., and Chakroun, W., "Surface roughness effects on flow over aerofoils," *Wind Engineering*, Vol. 21, January 1997, pp. 125–137.

[18] Lopes, L., and Burley, C., *ANOPP2 User's Manual: Version 1.2*, Hampton, VA, 2016.